



# OPEN Higgs decay and CP violation phase in the CPV TNMSSM

Ning-Yu Zhu , Hai-Xiang Chen & Huai-Cong Hu

In this study, we calculate the Higgs mass matrix and explore the limitations of the minimum conditions of the scalar potential on parameter degrees of freedom in the CP violation TNMSSM. We discuss the contributions of some parameters to Higgs mass, and their impact on the strength of Higgs decay signals in different decay channels  $h \rightarrow \gamma\gamma$ ,  $h \rightarrow VV$  ( $V = W, Z$ ) and  $h \rightarrow f\bar{f}$  ( $f = b, c, \tau$ ).

**Keywords** Supersymmetry, Higgs mass, CP violation, Higgs decays

The Standard Model (SM) of electroweak and strong interactions of elementary particles has achieved great success in the last century<sup>1,2</sup>. The Higgs particle was observed in 2012, which means that all particles in the SM have been discovered<sup>3,4</sup>. On the other hand, the SM also has some disadvantages, for example, its inability to explain neutrino oscillations<sup>5,6</sup> and the asymmetry of matter and antimatter in the universe, as well as can not provide the candidates for dark matter. Therefore, some extended models of SM have been proposed in an attempt to explain these issues.

The Minimal Supersymmetric Standard Model (MSSM) is a well-known new physics model<sup>7</sup>, which has been extensively studied by physicists in the past few decades. However, the MSSM also has some unexplained problems<sup>8</sup>, such as the hierarchical and  $\mu$  term problems, and physicists have proposed some extended models of the MSSM. The extension of the MSSM by addition a gauge singlet which is coupled to Higgs doublets (NMSSM) has been proposed to solve the  $\mu$  term problem<sup>9</sup>. The TNMSSM introduce a forbidden bare  $\mu$  term, and an effective  $\mu$  term is generated by the vacuum expectation value of the singlet. However, all the couplings in the NMSSM being perturbative up to the GUT scale also does not polish up the little gauge hierarchy problem<sup>10–15</sup>. Fortunately, the next-to-minimal supersymmetric standard model with triplets (TNMSSM) is proposed by Kautubh Agashe et al., which combines the advantages of NMSSM and TMSSM<sup>16,17</sup>. Compared with the MSSM, the TNMSSM introduces a gauge singlet and two  $SU(2)_L$  triplets with hypercharge  $Y = 0$ , which can validly solve the little gauge hierarchy and  $\mu$  term problems in MSSM. In addition, the TNMSSM can give neutrinos a small mass by introducing Majorana mass term without the need to introduce right-handed neutrinos<sup>16,18</sup>, which is cannot in the MSSM and NMSSM.

The violation of CP was first observed in neutral kaon decay experiments and strongly validated in B-meson decay experiments<sup>19,20</sup>. In addition to particle physics, CP violation (CPV) also provides a possible explanation for the asymmetry of matter and antimatter in the universe<sup>21</sup>. The Higgs interactions play an important role in mediating CPV, for example, CP is broken explicitly in the SM by complex Yukawa couplings of the Higgs boson to quarks. There are literatures indicating, in models that expand the Higgs sector, such as SUSY and MSSM, CP symmetries of those theories are broken spontaneously<sup>22,23</sup>.

The existence of Higgs boson has been confirmed, but further research is needed on its properties. In this paper, we consider the contributions of one-loop effective potential<sup>24</sup> and two-loop leading-log radiative correction<sup>25,26</sup> to Higgs mass, and calculate the mass matrix of Higgs boson in CPV TNMSSM and explore the reduction of parameter degrees of freedom by the minimum conditions of the scalar potential in Chapter II. The concrete theoretical expressions of Higgs decay are presented in Chapter III. It is found in the calculation that CPV appears in the tree level Higgs mass matrix in the CPV TNMSSM, which is absent in MSSM<sup>27</sup>. In numerical analysis, we find that the appearance of CPV in the tree level Higgs mass matrix has negative contributions to Higgs boson mass and greatly limits the range of parameter selection. Then we conduct a numerical analysis of the signal strength of Higgs decay in different decay channels in Chapter IV. We observe the effects of  $\tan\beta$ ,  $M\lambda$  (modulus of  $\lambda$ ),  $\tan\beta'$  and  $M\lambda_T$  (modulus of  $\lambda_T$ ) on signal strengths when  $\lambda_T$  and  $\chi_d$  were selected as different phase angles and  $M\chi_d$  (modulus of  $M\chi_d$ ) and  $\text{Re}A_u$  (real part of  $A_u$ ) were selected as different values. We note that because triplets have no coupling with fermions in the Lagrangian, the signal strengths of  $h \rightarrow f\bar{f}$  ( $f = b, c, \tau$ ) are almost unaffected when the phase angle of  $\lambda_T$  changes. In addition, in Chapter IV, we also calculate the electric dipole moments of neutrons and electrons, the contribution of doubly charged particles to Higgs decay, and the mass spectrum of doubly charged particles. In Chapter V, we discuss the results of the article.

Key Laboratory for Relativistic Astrophysics, School of Physical Science and Technology, Guangxi University, Nanning 530004, People's Republic of China. ✉email: hnzhu@163.com

## THE Higgs sector in the CPVTNMSSM The TNMSSM

Some literature has investigated B meson rare decays<sup>28</sup>, Higgs boson decays  $h \rightarrow MZ$ <sup>29</sup>, and transition magnetic moment of Majorana neutrinos<sup>18</sup> in the TNMSSM. These studies indicate that the TNMSSM is capable of making good predictions for B meson decay and neutrino transition magnetic moment, and provides valuable information for the experimental exploration of rare Higgs decays. In addition, M.A. Ouahid et al. studied the phenomenology of neutrinos and doubly charged Higgs in flavored-TNMSSM<sup>30</sup>.

Compared to the MSSM, the TNMSSM has an additional gauge singlet  $S$  and two  $SU(2)_L$  triplets  $T$  and  $\bar{T}$ . The superpotential of Higgs sector and Yukawa sector in TNMSSM are given as follows, respectively

$$W_{\text{Higgs}} = \lambda \hat{S} \hat{H}_u^T \cdot \hat{H}_d + \lambda_T \hat{S} \text{tr}(\hat{T} \hat{T}) + \frac{\kappa}{3} \hat{S}^3 + \chi_u \hat{H}_u^T \cdot \hat{T} \hat{H}_u + \chi_d \hat{H}_d^T \cdot \hat{T} \hat{H}_d, \quad (1)$$

$$W_{\text{Yukawa}} = h_u \hat{Q}^T \cdot \hat{H}_u \hat{U} - h_d \hat{Q}^T \cdot \hat{H}_d \hat{D} - h_l \hat{L}^T \cdot \hat{H}_d \hat{E}, \quad (2)$$

where  $\lambda, \lambda_T, \kappa, \chi_u$  and  $\chi_d$  are dimensionless. The field contents of the TNMSSM are given in Table 1. The singlet  $S$ , doublets  $H_u, H_d$  and triplets  $T, \bar{T}$  are given respectively by

$$H_u = (H_u^+, H_u^0), H_d = (H_d^0, H_d^-), \quad (3)$$

$$T = \begin{pmatrix} T^-/\sqrt{2} & -T^{--} \\ T^0 & -T^-/\sqrt{2} \end{pmatrix},$$

$$\bar{T} = \begin{pmatrix} \bar{T}^+/\sqrt{2} & -\bar{T}^0 \\ \bar{T}^{++} & -\bar{T}^+/\sqrt{2} \end{pmatrix}, \quad (4)$$

$$H_u^0 = (v_u + \phi_u + ia_u)/\sqrt{2}, H_d^0 = (v_d + \phi_d + ia_d)/\sqrt{2},$$

$$T^0 = (v_t + \phi_t + ia_t)/\sqrt{2}, S = (v_s + \phi_s + ia_s)/\sqrt{2},$$

$$\bar{T}^0 = (v_{\bar{t}} + \phi_{\bar{t}} + ia_{\bar{t}})/\sqrt{2},$$

where  $v_u, v_d, v_s, v_t$  and  $v_{\bar{t}}$  are vacuum expectation value (VEV) of singlet  $S$ , doublets  $H_u$  and  $H_d$ , triplets  $T$  and  $\bar{T}$ , respectively. Traditionally,  $\tan\beta$  and  $\tan\beta'$  are can defined by  $\tan\beta \equiv v_u/v_d$  and  $\tan\beta' \equiv v_t/v_{\bar{t}}$ . There is a relationship between VEV in SM and VEV in TNMSSM<sup>16</sup>

$$v^2 = v_u^2 + v_d^2 + 4v_t^2 + 4v_{\bar{t}}^2.$$

The soft supersymmetry-breaking Lagrangian reads

Superfields	Bosons	Fermions
$\hat{Q}$	$\tilde{Q}^T = (\tilde{u}, \tilde{d})_L$	$Q^T = (u, d)_L$
$\hat{L}$	$\tilde{L}^T = (\tilde{\nu}_l, \tilde{l})_L$	$L^T = (\nu_l, l)_L$
$\hat{U}$	$\tilde{U} = \tilde{u}_R^*$	$(u_R)^C = (u^C)_L$
$\hat{D}$	$\tilde{D} = \tilde{d}_R^*$	$(d_R)^C = (d^C)_L$
$\hat{E}$	$\tilde{E} = \tilde{l}_R^*$	$(l_R)^C = (l^C)_L$
$\hat{H}_u$	$H_u^T = (H_u^+, H_u^0)$	$\tilde{H}_u^T = (\tilde{H}_u^+, \tilde{H}_u^0)$
$\hat{H}_d$	$H_d^T = (H_d^0, H_d^-)$	$\tilde{H}_d^T = (\tilde{H}_d^0, \tilde{H}_d^-)$
$\hat{S}$	$S$	$\tilde{S}$
$\hat{T}$	$\begin{pmatrix} \tilde{T}^+/\sqrt{2} & -\tilde{T}^{++} \\ \tilde{T}^0 & -\tilde{T}^+/\sqrt{2} \end{pmatrix}$	$\begin{pmatrix} T^+/\sqrt{2} & -T^{++} \\ T^0 & -T^+/\sqrt{2} \end{pmatrix}$
$\hat{\bar{T}}$	$\begin{pmatrix} \tilde{\bar{T}}^-/\sqrt{2} & -\tilde{\bar{T}}^0 \\ \tilde{\bar{T}}^{--} & -\tilde{\bar{T}}^-/\sqrt{2} \end{pmatrix}$	$\begin{pmatrix} \bar{T}^-/\sqrt{2} & -\bar{T}^0 \\ \bar{T}^{--} & -\bar{T}^-/\sqrt{2} \end{pmatrix}$

**Table 1.** The field content of the TNMSSM.

$$\begin{aligned}
-\mathcal{L}_{\text{soft}} = & m_{H_u}^2 |H_u|^2 + m_{H_d}^2 |H_d|^2 + m_S^2 |S|^2 + m_T^2 \text{tr}(|T|^2) \\
& + m_{\tilde{T}}^2 \text{tr}|\tilde{T}|^2 + m_{\tilde{Q}}^2 |\tilde{Q}|^2 + m_{\tilde{U}}^2 |\tilde{U}|^2 + m_{\tilde{D}}^2 |\tilde{D}|^2 \\
& + m_{\tilde{L}}^2 |\tilde{L}|^2 + m_{\tilde{E}}^2 |\tilde{E}|^2 + (A_{h_u} \tilde{Q} \cdot H_u \tilde{U} \\
& - A_{h_d} \tilde{Q} \cdot H_d \tilde{D} - A_{h_l} \tilde{L} \cdot H_d \tilde{E} + A_{SH_u} \cdot H_d \\
& + A_T \text{Str}(T\tilde{T}) + \frac{A_k}{3} S^3 + A_u H_u \cdot \tilde{T} H_u \\
& + A_d H_d \cdot \tilde{T} H_d + h.c.) \\
& + \frac{1}{2} (M_1 \lambda_{\tilde{B}\tilde{B}} + M_2 \lambda_{\tilde{W}\tilde{W}} + M_3 \lambda_{\tilde{g}\tilde{g}} + h.c.).
\end{aligned} \tag{5}$$

## The potential and Higgs mass

In the supersymmetry theory, scalar supersymmetry potentials are given in the following way

$$V_0 = \frac{1}{2} D^a D^a + F_i^* F_i,$$

$F$  and  $D$  are two auxiliary functions

$$\begin{aligned}
F_i &= \partial W / \partial A_i, \\
D^a &= g A_i^* T_{ij}^a A_j.
\end{aligned}$$

In the  $\overline{\text{MS}}$  scheme, the CPV effective potential is determined by<sup>27</sup>

$$V_{\text{eff}} = V_0 + V_1,$$

$V_0$  is the tree level potential,  $V_1$  is the one-loop level effective potential with<sup>24</sup>

$$\begin{aligned}
V_1 = & \frac{3}{32\pi^2} \sum_{q=t,b,c} \left[ \sum_{i=1,2} m_{\tilde{q}_i}^4 \left( \ln \frac{m_{\tilde{q}_i}^2}{Q^2} - \frac{3}{2} \right) \right. \\
& \left. - 2m_q^4 \left( \ln \frac{m_q^2}{Q^2} - \frac{3}{2} \right) \right],
\end{aligned} \tag{6}$$

where  $m_q$  is the  $q$  quark mass, and  $m_{\tilde{q}}$  is the  $\tilde{q}$  squark mass and  $Q$  is the renormalization scale at TeV order. The mass matrix of squarks is given by

$$m_{\tilde{q}}^2 = \begin{pmatrix} m_{\tilde{q}_L \tilde{q}_L}^* & m_{\tilde{q}_R \tilde{q}_L}^* \\ m_{\tilde{q}_L \tilde{q}_R}^* & m_{\tilde{q}_R \tilde{q}_R}^* \end{pmatrix},$$

where the matrix elements for up-type squarks are

$$\begin{aligned}
m_{\tilde{u}_L \tilde{u}_L}^* &= \frac{1}{12} (g_1^2 - 3g_2^2) (H_u^{0,*} H_u^0 - H_d^{0,*} H_d^0 + 2H_T^{0,*} H_T^0 \\
& - 2H_{\tilde{T}}^{0,*} H_{\tilde{T}}^0) + \frac{1}{2} (2m_Q^2 + h_u^\dagger h_u H_u^{0,*} H_u^0), \\
m_{\tilde{u}_L \tilde{u}_R}^* &= A_{h_u} H_u^0 + h_u (2H_d^{0,*} H_T^{0,*} \chi_u^* - H_d^{0,*} H_s^{0,*} \lambda^*), \\
m_{\tilde{u}_R \tilde{u}_R}^* &= -\frac{1}{3} g_1^2 (H_u^{0,*} H_u^0 - H_d^{0,*} H_d^0 + 2H_T^{0,*} H_T^0 \\
& - 2H_{\tilde{T}}^{0,*} H_{\tilde{T}}^0) + \frac{1}{2} (2m_u^2 + h_u^\dagger h_u H_u^{0,*} H_u^0),
\end{aligned}$$

the matrix elements for down-type squarks are

$$\begin{aligned}
m_{\tilde{d}_L \tilde{d}_L}^* &= \frac{1}{12} (g_1^2 + 3g_2^2) (H_u^{0,*} H_u^0 - H_d^{0,*} H_d^0 + 2H_T^{0,*} H_T^0 \\
& - 2H_{\tilde{T}}^{0,*} H_{\tilde{T}}^0) + \frac{1}{2} (2m_Q^2 + h_d^\dagger h_d H_d^{0,*} H_d^0), \\
m_{\tilde{d}_L \tilde{d}_R}^* &= A_{h_d} H_d^0 + h_d (2H_u^{0,*} H_T^{0,*} \chi_d^* - H_u^{0,*} H_s^{0,*} \lambda^*), \\
m_{\tilde{d}_R \tilde{d}_R}^* &= \frac{1}{6} g_1^2 (H_u^{0,*} H_u^0 - H_d^{0,*} H_d^0 + 2H_T^{0,*} H_T^0 - 2H_{\tilde{T}}^{0,*} H_{\tilde{T}}^0) \\
& + \frac{1}{2} (2m_d^2 + h_d^\dagger h_d H_d^{0,*} H_d^0).
\end{aligned}$$

The mass of squarks can be obtained through

$$m_{\tilde{u}_{1,2}}^2 = \frac{1}{2} \left[ m_{\tilde{u}_L \tilde{u}_L} + m_{\tilde{u}_R \tilde{u}_R} \pm \sqrt{(m_{\tilde{u}_L \tilde{u}_L} - m_{\tilde{u}_R \tilde{u}_R})^2 - 4m_{\tilde{u}_L \tilde{u}_R} m_{\tilde{u}_R \tilde{u}_L}} \right],$$

$$m_{\tilde{d}_{1,2}}^2 = \frac{1}{2} \left[ m_{\tilde{d}_L \tilde{d}_L} + m_{\tilde{d}_R \tilde{d}_R} \pm \sqrt{(m_{\tilde{d}_L \tilde{d}_L} - m_{\tilde{d}_R \tilde{d}_R})^2 - 4m_{\tilde{d}_L \tilde{d}_R} m_{\tilde{d}_R \tilde{d}_L}} \right].$$

The elements of Higgs mass matrix can be calculated by the following formula on the basis  $(\phi_d, \phi_u, \phi_s, \phi_t, \phi_{\tilde{t}}, a_d, a_u, a_s, a_t, a_{\tilde{t}})$

$$m_{hij}^2 = \left\langle \frac{V_{eff}}{\phi_i \phi_j} \right|_{\phi_{ij} = \phi_d, \phi_u, \phi_s, \phi_t, \phi_{\tilde{t}}, a_d, a_u, a_s, a_t, a_{\tilde{t}}} \rangle.$$

It is found in the calculation that CPV appears in the tree level Higgs mass matrix in the CPV TNMSSM, namely  $m_{hij}$  and  $m_{hji} \neq 0$  ( $\phi_i = \phi_d, \phi_u, \phi_s, \phi_t, \phi_{\tilde{t}}$  and  $\phi_j = a_d, a_u, a_s, a_t, a_{\tilde{t}}$ ), which is absent in MSSM. In this paper, we consider the contributions of quarks (t,b,c) and squarks (stop, sbottom, scharm) to Higgs mass.

In addition, the Goldstone can be analytically obtained through  $Z^\dagger M_h Z$ , where  $Z$  is the unitary matrix defined as

$$Z = \frac{1}{v} \begin{pmatrix} v_{5 \times 5} & 0 & 0 & 0 & 0 & 0 \\ 0 & v_d & v_u & 0 & 2v_t & -2v_{\tilde{t}} \\ 0 & -v_u & v_d & 0 & 2v_{\tilde{t}} & 2v_t \\ 0 & 0 & 0 & v & 0 & 0 \\ 0 & -2v_t & -2v_{\tilde{t}} & 0 & v_d & -v_u \\ 0 & 2v_{\tilde{t}} & -2v_t & 0 & v_u & v_d \end{pmatrix}, \quad (7)$$

$$v_{5 \times 5} = \begin{pmatrix} v & 0 & 0 & 0 & 0 \\ 0 & v & 0 & 0 & 0 \\ 0 & 0 & v & 0 & 0 \\ 0 & 0 & 0 & v & 0 \\ 0 & 0 & 0 & 0 & v \end{pmatrix}.$$

Moreover, we also consider the contribution of two-loop radiative correction to the Higgs boson mass<sup>25,26,31</sup>

$$\Delta m_h^2 = \frac{3m_t^4}{4\pi^2 v^2} \left[ \frac{1}{16\pi^2} \left( \frac{3m_t^2}{2v^2} - 32\pi\alpha_3 \right) (\tilde{t}^2 + \tilde{X}_t \tilde{t}) \right]$$

$$\tilde{t} = \text{Log} \frac{M_S^2}{m_t^2}, \quad \tilde{X}_t = \frac{2\tilde{A}_t^2}{M_S} \left( 1 - \frac{\tilde{A}_t^2}{12M_S^2} \right) \quad (8)$$

where  $\alpha_3$  is the strong coupling constant,  $M_S = \sqrt{m_{\tilde{t}_1} m_{\tilde{t}_2}}$ ,  $\tilde{A}_t = A_{h_u} - |\mu| \cot \beta$ ,  $m_{\tilde{t}_1}$  and  $m_{\tilde{t}_2}$  denote the stop masses and  $A_{h_u}$  is the trilinear Higgs stop coupling.

Here we provide the mass matrices of doubly charged particles in TNMSSM. The mass matrix of the doubly charged Higgs  $m_{h^{\pm\pm}}$  is

$$m_{h^{\pm\pm}}^2 = \begin{pmatrix} m_{T^{--}T^{--,*}} & m_{T^{++,*}T^{--,*}} \\ m_{T^{--}T^{++}} & m_{T^{++,*}T^{++}} \end{pmatrix}. \quad (9)$$

where

$$m_{T^{--}T^{--,*}} = \frac{1}{2} v_s^2 |\lambda_T|^2 - \frac{1}{4} (g_1^2 - g_2^2) (v_u^2 - v_d^2 + 2v_t^2 - 2v_{\tilde{t}}^2) + m_{\tilde{t}}^2,$$

$$m_{T^{--}T^{++}} = \frac{1}{2} (\lambda_T (v_u v_d \lambda^* + v_t v_{\tilde{t}} \lambda_T) - (v_s \lambda_T k^* + \sqrt{2} A_T)),$$

$$m_{T^{++,*}T^{++}} = \frac{1}{2} v_s^2 |\lambda_T|^2 - \frac{1}{4} (g_1^2 - g_2^2) (v_u^2 - v_d^2 + 2v_t^2 - 2v_{\tilde{t}}^2) + m_{\tilde{t}}^2.$$

The mass matrix of the doubly chargino  $m_{\chi^{\pm\pm}}$  is

$$m_{\chi^{\pm\pm}\chi^{\pm\pm}} = \frac{1}{\sqrt{2}} v_s |\lambda_T|. \quad (10)$$

### CP violation and phase angle

Consider  $Ae^{i\theta_A}Be^{i\theta_B}Ce^{i\theta_C}$  is a term in Lagrangian,  $A, B, C$  are parameters or fields in Lagrangian, because  $ABCe^{i(\theta_A+\theta_B+\theta_C)} = Ae^{i\theta_A}Be^{i\theta_B}Ce^{i\theta_C}$ , we can absorb all the phase angles of the fields into the coupling coefficient through redefining  $e^{i\theta_i} = e^{i\theta_A}e^{i\theta_B}e^{i\theta_C}$ . Because all phase angles are undetermined, it is sufficient and reasonable to only add phase angles to the coupling coefficient. In this paper, we use  $MA_ie^{i\theta_i}$  to represent complex parameters  $A_i$ ,  $MA_i$  is modulus of complex parameters  $A_i$ .

The total tadpoles are given by:

$$T_{\phi_i} = \left\langle \frac{V_{\text{eff}}}{\phi_i} \right\rangle = T_{\phi_i}^0 + T_{\phi_i}^1, \quad (11)$$

$$\phi_i = \phi_d, \phi_u, \phi_s, \phi_t, \phi_{\bar{t}}, a_d, a_u, a_s, a_t, a_{\bar{t}},$$

where

$$T_{\phi_i}^0 = \left\langle \frac{V_0}{\phi_i} \Big|_{\phi_i=\phi_d, \phi_u, \phi_s, \phi_t, \phi_{\bar{t}}, a_d, a_u, a_s, a_t, a_{\bar{t}}} \right\rangle$$

$$T_{\phi_i}^1 = \left\langle \frac{V_1}{\phi_i} \Big|_{\phi_i=\phi_d, \phi_u, \phi_s, \phi_t, \phi_{\bar{t}}, a_d, a_u, a_s, a_t, a_{\bar{t}}} \right\rangle,$$

$T_{\phi_i}^0$  and  $T_{\phi_i}^1$  are given in the appendix A. Due to the requirement of vanishing tadpole equations, the degrees of freedom of the parameters can be reduced, i.e.  $m_i^2$  ( $i = H_u, H_d, S, T$  and  $\bar{T}$ ) disappear in the main diagonal elements of the Higgs mass matrix, and the imaginary parts of the five parameters  $A_i$  ( $A_i = A_u, A_d, A_k, A_T, A_{H_u}$ ) will be reduced. The reduced imaginary parts of those parameters are present in the appendix A (A1–A5).

### THE 125 Higgs decays

The Higgs boson is a mixed state of CP-even and CP-odd components in CPV theory, differentiate from the SM Higgs boson, both of the two final states appear and could be distinguished from each other by detecting photon polarization<sup>32</sup>.

The Higgs are mainly produced by gluon pairs fusion in LHC experiments<sup>33,34</sup>. The one loop diagrams with virtual top quarks have the most significant contribution to the leading order (LO). In new physics (NP), one-loop diagrams containing virtual squarks also contribute to the LO. In this section, we use  $H$  to denote CP-even Higgs and  $A$  to denote CP-odd Higgs. The decay widths of CP-even Higgs to gluon pairs  $H \rightarrow gg$  and CP-odd Higgs to gluon pairs  $A \rightarrow gg$  are given respectively by<sup>35–40</sup>:

$$\Gamma_{\text{NP}}(H \rightarrow gg) = \frac{G_F \alpha_s^2 m_H^3}{64 \sqrt{2} \pi^3} \left| \sum_q g_{Hqq} A_{1/2}^H(x_q) + \sum_{\tilde{q}} g_{H\tilde{q}\tilde{q}} \frac{m_Z^2}{m_{\tilde{q}}^2} A_0^H(x_{\tilde{q}}) \right|^2, \quad (12)$$

$$\Gamma_{\text{NP}}(A \rightarrow gg) = \frac{G_F \alpha_s^2 m_A^3}{64 \sqrt{2} \pi^3} \left| \sum_q g_{Aqq} A_{1/2}^A(x_q) \right|^2 \quad (13)$$

The LO contributions to the decay Higgs to diphoton come from the one-loop diagrams. In the NP, all of the fermions,  $W$  boson and these supersymmetric partners contribute to Higgs to diphoton decay. The partial widths of CP-even Higgs and CP-odd Higgs bosons decay into diphoton are given by<sup>33,41–46</sup>:

$$\begin{aligned}
\Gamma_{\text{NP}}(H \rightarrow \gamma\gamma) = & \frac{G_F \alpha_s^2 m_H^3}{128 \sqrt{2} \pi^3} \left| \sum_f N_c Q_f^2 g_{Hff} A_{1/2}^H(x_f) \right. \\
& + \sum_{\tilde{f}} N_c Q_{\tilde{f}}^2 g_{H\tilde{f}\tilde{f}} \frac{m_Z^2}{m_{\tilde{f}}^2} A_0^H(x_{\tilde{f}})^2 \\
& + \sum_{i=1}^3 g_{HH_i^+ H_i^-} \frac{m_Z^2}{m_{H_i^\pm}^2} A_0^H(x_{H_i^\pm}) \\
& + \sum_{j=1}^2 Q_{H_j^{++}}^2 g_{HH_j^{++} H_j^{--}} \frac{m_Z^2}{m_{H_j^{\pm\pm}}^2} A_0^H(x_{H_j^{\pm\pm}}) \\
& + \sum_{k=1}^3 g_{H\chi_k^+ \chi_k^-} \frac{m_W}{m_{\chi_k^\pm}^2} A_{1/2}^H(x_{\chi_k^\pm}) \\
& + Q_{\chi^{++}}^2 g_{H\chi^{++} \chi^{--}} \frac{m_W}{m_{\chi^{\pm\pm}}^2} A_{1/2}^H(x_{\chi^{\pm\pm}}) \\
& \left. + g_{HWW} A_1^H(x_W) \right|^2,
\end{aligned} \tag{14}$$

$$\begin{aligned}
\Gamma_{\text{NP}}(A \rightarrow \gamma\gamma) = & \frac{G_F \alpha_s^2 m_A^3}{128 \sqrt{2} \pi^3} \left| \sum_f N_c Q_f^2 g_{Aff} A_{1/2}^A(x_f) \right. \\
& + \sum_{k=1}^3 g_{A\chi_k^+ \chi_k^-} \frac{m_W^2}{m_{\chi_k^\pm}^2} A_{1/2}^A(x_{\chi_k^\pm}) \\
& \left. + Q_{\chi^{++}}^2 g_{A\chi^{++} \chi^{--}} \frac{m_W^2}{m_{\chi^{\pm\pm}}^2} A_{1/2}^A(x_{\chi^{\pm\pm}}) \right|^2,
\end{aligned} \tag{15}$$

where  $x_i = m_h^2/(4m_i^2)$ ,  $A_1^H(x)$ ,  $A_{\frac{1}{2}}^H(x)$ ,  $A_0^H(x)$  and  $g(x)$  are given by<sup>47</sup>

$$\begin{aligned}
A_1^H(x) &= -[2x^2 + 3x + 3(2x - 1)g(x)]/x^2, \\
A_{\frac{1}{2}}^H(x) &= 2[x + (x - 1)g(x)]/x^2, \\
A_0^H(x) &= -(x - g(x))/x^2, \\
A_{1/2}^A(x) &= 2g(x)/x, \\
g(x) &= \begin{cases} \arcsin^2 \sqrt{x}, & x \leq 1 \\ -\frac{1}{4} \left[ \ln \frac{1+\sqrt{1-1/x}}{1-\sqrt{1-1/x}} - i\pi \right]^2, & x > 1 \end{cases}
\end{aligned} \tag{16}$$

The partial widths of CP-even Higgs bosons decay into vector boson pairs  $H \rightarrow VV$  ( $V = W, Z$ ) are given by<sup>48–55</sup>:

$$\Gamma_{\text{NP}}(H \rightarrow WW) = \frac{3e^4 m_H}{512 \pi^3 s_W^4} |g_{HWW}|^2 F\left(\frac{m_W}{m_H}\right), \tag{17}$$

$$\begin{aligned}
\Gamma_{\text{NP}}(H \rightarrow ZZ) = & \frac{e^4 m_H}{2048 \pi^3 s_W^4 c_W^4} \left( 7 - \frac{40}{3} s_W^2 + \frac{160}{9} s_W^4 \right) \\
& \times |g_{HZZ}|^2 F\left(\frac{m_Z}{m_H}\right),
\end{aligned} \tag{18}$$

with

$$\begin{aligned}
F(x) = & -(1 - x^2) \left( \frac{47}{2} x^2 - \frac{13}{2} + \frac{1}{x^2} \right) \\
& - 3(1 - 6x^2 + 4x^4) \ln x \\
& + \frac{3(1 - 8x^2 + 20x^4)}{\sqrt{4x^2 - 1}} \arccos\left(\frac{3x^2 - 1}{2x^3}\right)
\end{aligned}$$

CP-odd Higgs A is uncoupled with vector bosons in tree-level.

In the Born approximation, the partial decay widths of CP-even and CP-odd Higgs bosons decay into fermion pairs are given by<sup>35,49</sup>:

$$\Gamma_{\text{NP}}(H \rightarrow f\bar{f}) = \frac{N_c G_F m_f^2 m_H}{4\sqrt{2}\pi} |g_{Hff}|^2 \beta_f^3, \quad (19)$$

$$\Gamma_{\text{NP}}(A \rightarrow f\bar{f}) = \frac{N_c G_F m_f^2 m_A}{4\sqrt{2}\pi} |g_{Aff}|^2 \beta_f, \quad (20)$$

$$\beta_f = \left(1 - \frac{4m_f^2}{m_{H,A}^2}\right)^{\frac{1}{2}}$$

In the CPV TNMSSM, the concrete expressions for  $g_{Hff}$ ,  $g_{H\tilde{f}\tilde{f}}$ ,  $g_{HH^+H^-}$ ,  $g_{HH^{++}H^{--}}$ ,  $g_{H\chi^+\chi^-}$ ,  $g_{H\chi^{++}\chi^{--}}$ ,  $g_{HVV}$ ,  $g_{Aff}$ ,  $g_{A\chi^+\chi^-}$  and  $g_{A\chi^{++}\chi^{--}}$  appeared in Eqs. (6–9, 11–14) are given in the appendix B.

The signal strengths for the Higgs decay channels are<sup>56</sup>

$$\mu_{\gamma\gamma, VV}^{\text{ggF}} = \frac{\sigma_{\text{NP}}(\text{ggF})}{\sigma_{\text{SM}}(\text{ggF})} \frac{BR_{\text{NP}}(h \rightarrow \gamma\gamma, VV)}{BR_{\text{SM}}(h \rightarrow \gamma\gamma, VV)}, (V = W, Z) \quad (21)$$

$$\mu_{f\bar{f}}^{\text{VBF}} = \frac{\sigma_{\text{NP}}(\text{VBF})}{\sigma_{\text{SM}}(\text{VBF})} \frac{BR_{\text{NP}}(h \rightarrow f\bar{f})}{BR_{\text{SM}}(h \rightarrow f\bar{f})}, (f = b, c, \tau)$$

The Higgs production cross sections can be simplified through

$$\frac{\sigma_{\text{NP}}(\text{ggF})}{\sigma_{\text{SM}}(\text{ggF})} \approx \frac{\Gamma_{\text{NP}}(h \rightarrow \text{gg})}{\Gamma_{\text{SM}}(h \rightarrow \text{gg})},$$

$$\frac{\sigma_{\text{NP}}(\text{VBF})}{\sigma_{\text{SM}}(\text{VBF})} \approx \frac{\Gamma_{\text{NP}}(h \rightarrow VV)}{\Gamma_{\text{SM}}(h \rightarrow VV)},$$

the ratios of the signal strengths from the Higgs decay channels can be reduced as

$$\mu_{\gamma\gamma}^{\text{ggF}} = \frac{\Gamma_{\text{SM}}}{\Gamma_{\text{NP}}} \frac{\Gamma_{\text{NP}}(h \rightarrow \text{gg})}{\Gamma_{\text{SM}}(h \rightarrow \text{gg})} \frac{\Gamma_{\text{NP}}(h \rightarrow \gamma\gamma)}{\Gamma_{\text{SM}}(h \rightarrow \gamma\gamma)}$$

$$\mu_{VV}^{\text{ggF}} = \frac{\Gamma_{\text{SM}}}{\Gamma_{\text{NP}}} \frac{\Gamma_{\text{NP}}(h \rightarrow \text{gg})}{\Gamma_{\text{SM}}(h \rightarrow \text{gg})} \frac{\Gamma_{\text{NP}}(h \rightarrow VV)}{\Gamma_{\text{SM}}(h \rightarrow VV)} \quad (22)$$

$$\mu_{f\bar{f}}^{\text{VBF}} = \frac{\Gamma_{\text{SM}}}{\Gamma_{\text{NP}}} \frac{\Gamma_{\text{NP}}(h \rightarrow VV)}{\Gamma_{\text{SM}}(h \rightarrow VV)} \frac{\Gamma_{\text{NP}}(h \rightarrow f\bar{f})}{\Gamma_{\text{SM}}(h \rightarrow f\bar{f})},$$

where  $\Gamma_{\text{NP}} = \sum_f \Gamma_{\text{NP}}(h \rightarrow f\bar{f}) + \sum_V \Gamma_{\text{NP}}(h \rightarrow VV) + \Gamma_{\text{NP}}(h \rightarrow \text{gg}) + \Gamma_{\text{NP}}(h \rightarrow \gamma\gamma)$ , represents the NP total decay width of physical Higgs.

## Numerical analysis

We study the mass and decay of the lightest Higgs boson  $h^0$  in CPV TNMSSM in this section. After considering the experimental limitations, the scalar lepton masses larger than 700 GeV, and chargino masses larger than 1100 GeV<sup>57</sup>, the parameters in CPV TNMSSM were selected as

$$\begin{aligned} v_s &= 1 \text{ TeV}, M_1 = 1 \text{ TeV}, M_2 = 1 \text{ TeV}, \\ Q &= 1 \text{ TeV}, Mk = 0.9, M_{\chi_u} = 0.3, \\ MA &= 0.8 \text{ TeV}, \theta_\lambda = 0.02, \theta_k = 0.05, \\ \theta_{\chi_u} &= \pi/3, \theta_A = 0.01, \text{Re}A_d = 0.5 \text{ TeV}, \\ \text{Re}A_k &= -0.5 \text{ TeV}, \text{Re}A_T = 0.5 \text{ TeV}, \\ A_{h_d} &= A_{h_l} = \text{Re}A_{h_u} = 0.2 \text{ TeV}, \\ m_Q^2 &= m_u^2 = m_d^2 = m_L^2 = m_e^2 = 1.8 \text{ TeV}^2. \end{aligned} \quad (23)$$

where  $\text{Re}A_i$  are the real parts of  $A_i$  ( $A_i = A_u, A_d, A_k, A_T, A_{h_u}$ ),  $M_{A_j}$  are the modulus of  $A_j$  ( $A_j = \lambda_T, k, \chi_u, \chi_d, A$ ), and  $\theta_{A_k}$  are the CP phase of  $A_k$  ( $A_k = \lambda, k, \chi_u, A$ ), respectively.

Due to the CP violation appears in the tree-level Higgs mass matrix which leads to a negative contribution to Higgs mass and the value of  $v_s$  is large, the selection ranges of phase angles for  $\lambda, k$  and  $A$  are strictly limited.

From the superpotential equations (1) and (2), it can be simply inferred that due to the vacuum expectation value  $v_t$  and  $v_{\tilde{t}}$  are very small compared to the vacuum expectation value  $v_u, v_d$  and  $v_s$ , the parameters that have no coupling with  $S, H_u$  and  $H_d$  are not sensitive to the influence of higgs mass and decay signal strengths. Moreover, because of the value of  $v_s$  is very large, some parameters such as  $\chi_u, k, A$  and  $A_k$  are too sensitive to higgs mass, resulting in the inability to observe those impacts on the decay signal strengths within suitable parameter ranges. After considering the above factors, we select the parameters that are sensitive to signal strengths and analyse the results.

We adopt the parameters as follow

$$\begin{aligned}
 6 \leq \tan\beta \leq 50, \quad 0.2 \leq M\lambda \leq 0.6, \\
 0.3 \leq \tan\beta' \leq 6, \quad 0.35 \leq M\lambda_T \leq 1, \\
 \theta_{\lambda_T} = 0, \pi/4, \pi/3 \text{ and } \pi/2, \\
 \theta_{\chi_d} = 0, \pi/3, \pi/2, \pi, \\
 M\chi_d = 0.5, 0.6, 0.7, 0.8, \\
 \text{Re}A_u = -400, -500, -600, -700,
 \end{aligned}
 \quad (24)$$

We explore the effects of these parameters on the Higgs mass and consider the limitations of experiments on Higgs mass, further explore their effects on Higgs decay signal strengths. In Figs. 1, 3 and 5, we adopt  $\tan\beta' = 1.5$ ,  $M\lambda_T = 0.9$ ,  $M\chi_d = 0.8$  and  $\text{Re}A_u = -500$ , in Figs. 2, 4 and 6, we adopt  $\tan\beta = 10$ ,  $\theta_{\lambda_T} = \pi/6$ ,  $M\lambda = 0.4$  and  $\theta_{\chi_d} = 0.8$ .

In Fig. 1a and b, we select  $M\lambda = 0.4$ ,  $\theta_{\chi_d} = \pi/3$  when observing the effects of  $\tan\beta$  and  $\theta_{\lambda_T}$  on  $h^0$  mass, select  $\tan\beta = 10$ ,  $\theta_{\lambda_T} = \pi/6$  when observing the effects of  $M\lambda$  and  $\theta_{\chi_d}$  on  $h^0$  mass. In Fig. 2a and b, we select  $M\lambda_T = 0.9$ ,  $\text{Re}A_u = -500$  when observing the effects of  $\tan\beta'$  and  $M\chi_d$  on  $h^0$  mass, select  $\tan\beta' = 1.5$ ,  $M\chi_d = 0.8$  when observing the effects of  $M\lambda_T$  and  $\text{Re}A_u$  on  $h^0$  mass.

We take the parameter ranges to accept  $124 \text{ GeV} \leq m_{h^0} \leq 126.5 \text{ GeV}$  and study the impacts of these two sets of parameters on signal strengths. After considering the experimental data of Higgs mass, these parameter spaces are further limited

$$\begin{aligned}
 8 \leq \tan\beta \leq 50, \quad 0.35 \leq M\lambda \leq 0.55, \\
 0.5 \leq \tan\beta' \leq 5, \quad 0.45 \leq M\lambda_T \leq 0.8,
 \end{aligned}
 \quad (25)$$

We analyse signal strengths within the new parameter ranges.

In addition, the selection of complex parameters, especially the phase angle, is strongly limited by the electric dipole moments (EDM) of electrons and neutrons. To further verify the rationality of these parameters, we calculated the electric dipole moments of electrons and neutrons using some unique parameters of TNMSSM. These results are presented in Figs. 3 and 4.

The effective Lagrangian for spin- $\frac{1}{2}$  particles EDMs can be written as

$$\mathcal{L}_I^{\text{EDM}} = -\frac{i}{2} d_f \bar{\psi} \sigma_{\mu\nu} \gamma_5 \psi F^{\mu\nu}$$

Similarly, the effective Lagrangian for spin- $\frac{1}{2}$  particles EDMs can be written as

$$\mathcal{L}_I^{\text{CEDM}} = -\frac{i}{2} \tilde{d}_q^C \bar{q} \sigma_{\mu\nu} \gamma_5 T^a q G^{\mu\nu a}.$$

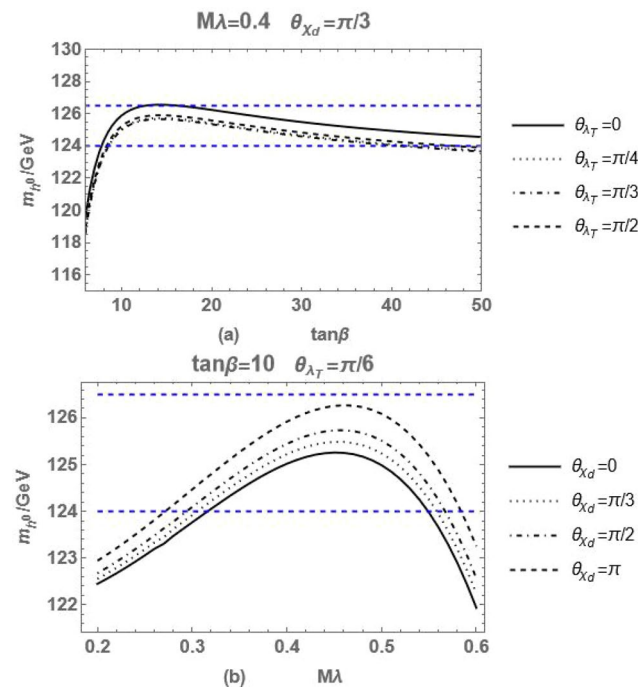


**Fig. 1.** (a) The variation of the mass of  $h^0$  with  $\tan\beta$  when  $\theta_{\lambda_T}$  is selected as different phase angles. (b) The variation of the mass of  $h^0$  with  $M\lambda$  when  $\theta_{\chi_d}$  is selected as different phase angles.



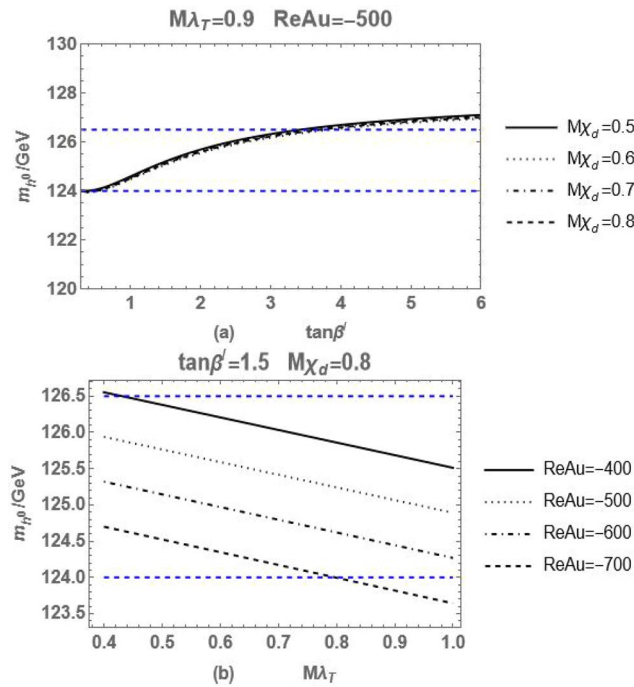


**Fig. 2.** (a) The variation of the mass of  $h^0$  with  $\tan\beta'$  when  $M\chi_d$  is selected as different values. (b) The variation of the mass of  $h^0$  with  $M\lambda_T$  when  $\text{Re}A_u$  is selected as different values.

The concrete formulas of EDMs and CEDMs can be seen in<sup>58–62</sup>. The research by T.Ibrahim et al. shows that the main factors affecting fermion EDM are the phase of the fermion field, vector Superfields, Higgs field, and the coupling parameters between Higgs fields<sup>58</sup>. Due to the fact that this article only considers the phase of parameters related to Higgs decay, and  $\lambda$  and  $\chi_u$  have already been selected, only the phase of  $\chi_d$  and  $\lambda_T$  needs to be considered.

The experimental limitations for neutron and electron EDM are  $d_n < 0.18 \times 10^{25}$  and  $d_e < 0.11 \times 10^{28}$ , respectively, which are denoted by blue dashed lines in the Figs. 3 and 4. Due to the influence of  $\lambda$  and  $\chi_u$  not being equal to 0, the EDM of electrons and neutrons is not equal to 0 when  $\chi_d$  and  $\lambda_T$  are equal to 0. When  $\lambda_T$  changes, the EDM of electrons and neutrons does not change. This is because singlet and triplets are not coupled with fermions. The calculation results are in good agreement with experimental limits, leading us to believe that these parameters are appropriate.

When different phase angles for  $\lambda_T$  and  $\chi_d$  are selected,  $\mu_{\gamma\gamma}^{ggF}$  in Fig. 5a and b first increases and then decreases, and reaches its maximum at  $\tan\beta = 12$  and  $M\lambda = 0.47$ ,  $\mu_{VV}^{ggF}$  in Fig. 5a and d first increases and then decreases, and reaches its maximum at  $\tan\beta = 14$  and  $M\lambda = 0.46$ , respectively. According to the data provided in PDG<sup>57</sup>,  $\mu_{\gamma\gamma}^{exp} = 1.10 \pm 0.07^{63–66}$ ,  $\mu_{WW}^{exp} = 1.19 \pm 0.12^{65,66}$ ,  $\mu_{ZZ}^{exp} = 1.01 \pm 0.07^{65,67,68}$ , the maximum error between the experimental data and the theoretical prediction of  $\mu_{\gamma\gamma}$  is about  $1\sigma$  and of  $\mu_{WW}$  is less than  $1\sigma$  and of  $\mu_{ZZ}$  is approaching  $2.5\sigma$ .

When different values for  $M\chi_d$  and  $\text{Re}A_u$  are selected,  $\mu_{\gamma\gamma}^{ggF}$  gradually increasing in Fig. 6a and gradually decreasing in Fig. 6b,  $\mu_{VV}^{ggF}$  gradually increasing in Fig. 6c and gradually decreasing in Fig. 6d, respectively. Because the value of  $v_d$  is relatively small compared to  $v_u$  when  $\tan\beta=10$ , the effects of  $M\chi_d$  on signal strengths are insensitive, so that  $\mu_{\gamma\gamma}^{ggF}$  and  $\mu_{VV}^{ggF}$  remain almost unchanged when  $M\chi_d$  changes. According to the data provided in PDG, the maximum error between the experimental data and the theoretical prediction of  $\mu_{\gamma\gamma}$  is about  $1.1\sigma$  and of  $\mu_{WW}$  is less than  $0.8\sigma$  and of  $\mu_{ZZ}$  is approaching  $2.4\sigma$ .

When different phase angles for  $\lambda_T$  and  $\chi_d$  are selected,  $\mu_{bb}^{VBF}$  and  $\mu_{\tau\tau}^{VBF}$  in Fig. 7a and b gradually decreasing,  $\mu_{cc}^{VBF}$  in Fig. 7c and d gradually increasing. According to the data provided in PDG<sup>57</sup>,  $\mu_{bb}^{exp} = 0.98 \pm 0.12^{65,66,69,70}$ ,  $\mu_{cc}^{exp} = 37 \pm 20^{71,72}$ , and  $\mu_{\tau\tau}^{exp} = 1.15_{-0.15}^{+0.16,65,66,73}$ , the maximum error between the experimental data and the theoretical prediction of  $\mu_{bb}$  is about  $1.6\sigma$ , of  $\mu_{cc}$  is less than  $1.5\sigma$  and of  $\mu_{\tau\tau}$  is much less than  $1\sigma$ . When different phase angles of  $\lambda_T$  are selected,  $\mu_{bb}^{VBF}$ ,  $\mu_{\tau\tau}^{VBF}$  and  $\mu_{cc}^{VBF}$  remain almost unchanged, because the Higgs singlet and triplets are uncoupled with fermions in the Lagrangian.

When different values for  $M\chi_d$  and  $\text{Re}A_u$  are selected,  $\mu_{\gamma\gamma}^{ggF}$  almost unchanged in Fig. 8a and b,  $\mu_{VV}^{ggF}$  almost unchanged in Fig. 8d and only slightly reduce in Fig. 8c. This meets our expectation because these parameters are uncoupled with fermions in the Lagrangian.

We calculated  $\Gamma_{NP}(h \rightarrow \gamma\gamma)$  after ignoring the contribution of doubly charged particles  $\Gamma_{NP}^{no\ doubly}(h \rightarrow \gamma\gamma)$  and compared it with  $\Gamma_{NP}(h \rightarrow \gamma\gamma)$  to quantify the contribution of two charged particles to the decay  $h \rightarrow \gamma\gamma$ . These results are presented in Fig. 9. The  $C_{doubly}$  in Fig. 9 is defined by

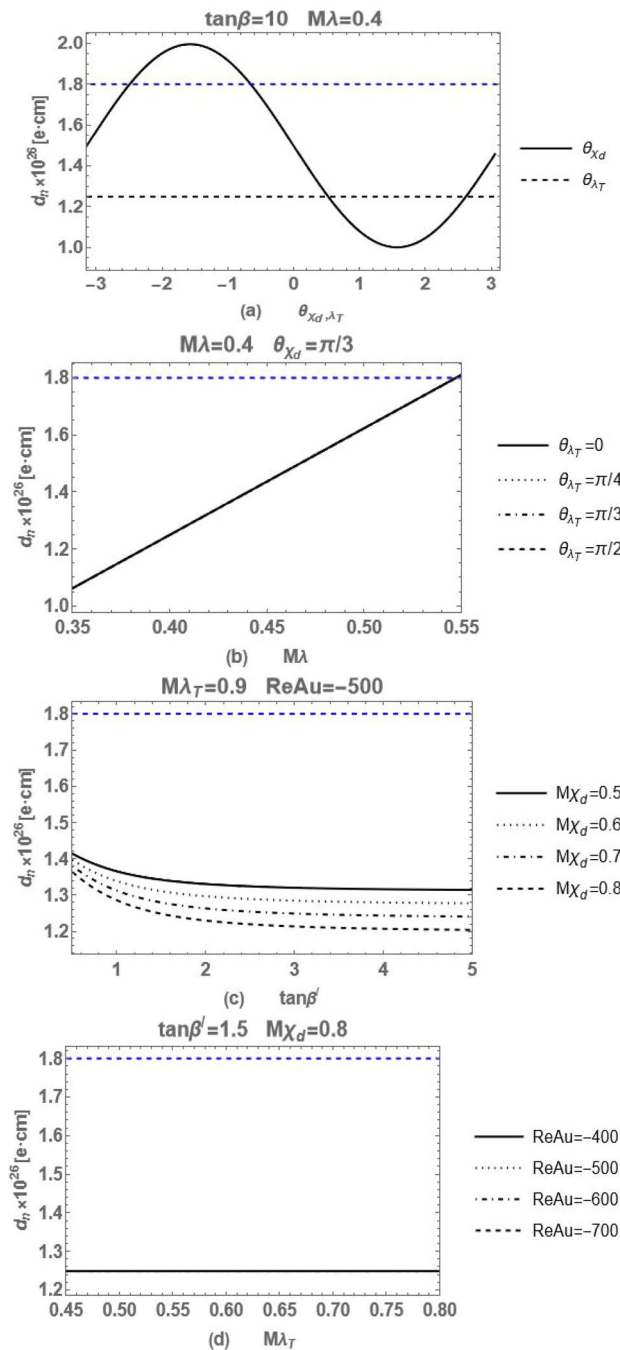


**Fig. 3.** (a) The variation of neutron EDM with  $\theta_{\chi_d}$  and  $\theta_{\lambda_T}$ . (b) The variation of neutron EDM with  $M\lambda$  when  $\theta_{\lambda_T}$  is selected as different values. (c) the variation of neutron EDM with  $\tan\beta'$  when  $M\chi_d$  is selected as different values. (d) The variation of neutron EDM with  $M\lambda_T$  when  $\text{Re}A_u$  is selected as different values.

$$C_{\text{doubly}} = \frac{\Gamma_{\text{NP}}(h \rightarrow \gamma\gamma) - \Gamma_{\text{NP}}^{\text{no doubly}}(h \rightarrow \gamma\gamma)}{\Gamma_{\text{NP}}(h \rightarrow \gamma\gamma)}.$$

Due to the large mass of the doubly charged Higgs, its contribution to the decay width is small. For the doubly charged chargino, because the vacuum expectation values of triplets are very small, its contribution to the decay width is also small.

We calculate the masses of the lightest doubly charged Higgs boson  $h^{++}$  and doubly charged chargino  $\chi^{++}$ , and compared them with experimental results. The analytical expressions for the mass of doubly charged Higgs boson and doubly charged chargino are given in Eqs. (9) and (10), and the numerical results are shown in Figs. 10 and 11.

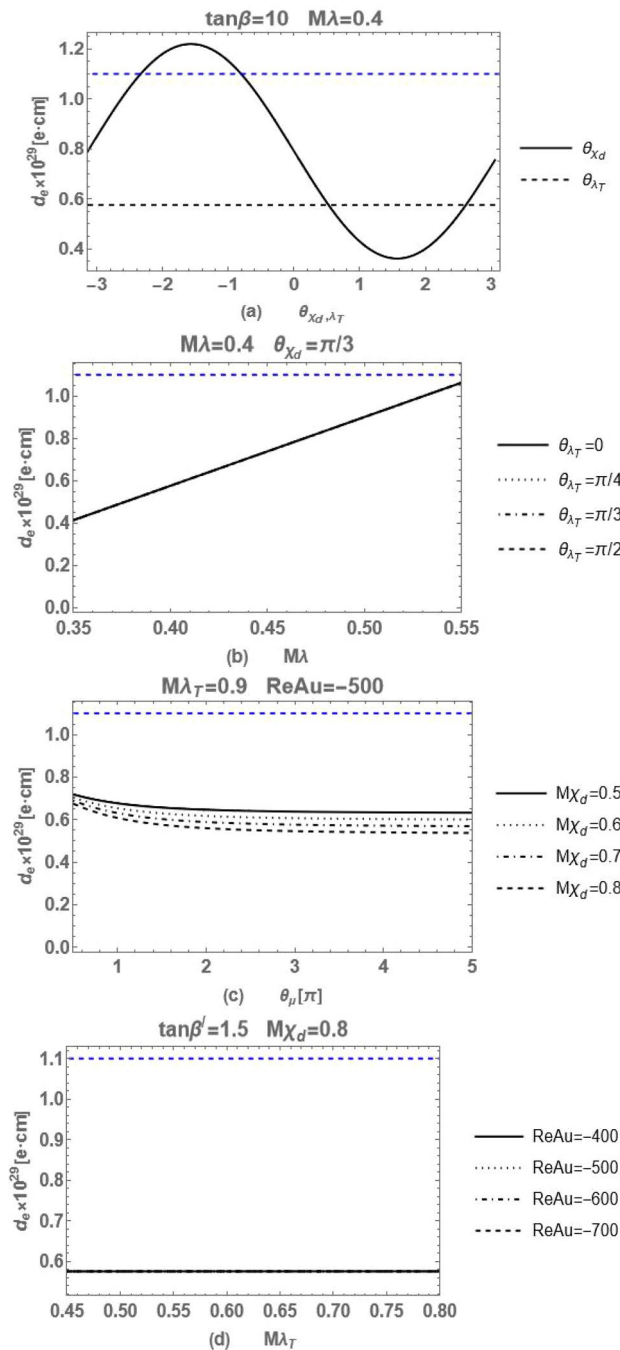


**Fig. 4.** (a) The variation of electron EDM with  $\theta_{\chi_d}$  and  $\theta_{\lambda_T}$ . (b) The variation of electron EDM with  $M\lambda$  when  $\theta_{\lambda_T}$  is selected as different values. (c) The variation of electron EDM with  $\tan\beta'$  when  $M\chi_d$  is selected as different values. (d) The variation of electron EDM with  $M\lambda_T$  when  $\text{Re}Au$  is selected as different values.

The limitation of the experiment is that  $m_{h^{++}} > 1080 \text{ GeV}^{74-76}$ , we mark it with a blue dashed line in the Fig. 10. From the Eq. (10), it can be seen that the mass of  $m_{\chi^{++}}$  depends only on  $\lambda_T$ .

## Conclusion

As an extended model of MSSM, the TNMSSM introduces a new gauge singlet  $S$  and two  $SU(2)_L$  triplets  $T, \bar{T}$ . The neutral parts of Higgs singlet, two Higgs doublets ( $H_d$  and  $H_u$ ) and two Higgs singlets mix together, which constitute a  $10 \times 10$  mass squared matrix of Higgs boson after considering CP violation. After considering the contributions of one-loop effective potential and two-loop radiative correction, we obtain complete Higgs mass matrix and the lightest Higgs  $h^0$  with a mass  $m_{h^0}$  near 125 GeV in Chapter II. We show concrete theoretical expressions of the Higgs decay in Chapter III, and provide the concrete expressions of  $g_{Hff}, g_{H\tilde{f}\tilde{f}}, g_{HH^+H^-}, g_{HH^{++}H^{--}}, g_{H\chi^+\chi^-}, g_{H\chi^+\chi^-}, g_{HVV}, g_{Aff}, g_{A\chi^+\chi^-}$  and  $g_{A\chi^+\chi^-}$  in the appendix B.

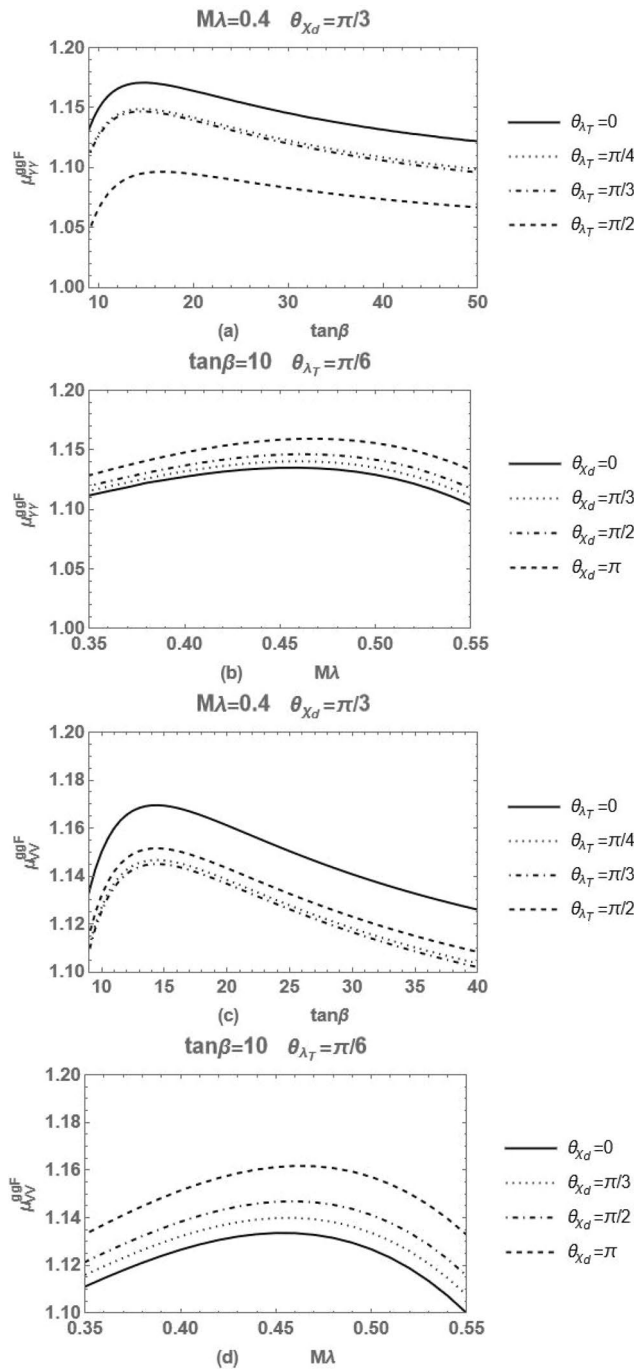


**Fig. 5.** (a, b) The variation of the signal strength  $\mu_{\gamma\gamma}^{ggF}$  and  $\mu_{\gamma\gamma}^{VBF}$  with  $\tan\beta$  when  $\theta_{\lambda_T}$  is selected as different phase angles. (c, d) The variation of the signal strength  $\mu_{\gamma\gamma}^{ggF}$  and  $\mu_{\gamma\gamma}^{VBF}$  with  $M\lambda$  when  $\theta_{\chi_d}$  is selected as different phase angles.

We explore the limitations of the minimum conditions of the scalar potential on the degrees of freedom of parameters and present the relevant results in the appendix A. After considering the minimum conditions of the scalar potential in the CPV TNMSSM model, we reduce five parameters  $m_i^2$  ( $i = H_u, H_d, S, T$  and  $\bar{T}$ ) and the imaginary parts of the five parameters  $A_i$  ( $A_i = A_u, A_d, A_k, A_T, A_{h_u}$ ). In Chapter IV, after considering limitations of the minimum conditions of the scalar potential and Higgs mass, we obtain a set of parameters and calculate the signal strengths of Higgs decay in different decay channels  $h \rightarrow \gamma\gamma$ ,  $h \rightarrow VV$  ( $V = W, Z$ ) and  $h \rightarrow f\bar{f}$  ( $f = b, c, \tau$ ), and compare them with experimental results in PDG, where  $\mu_{\gamma\gamma}^{VBF}$ ,  $\mu_{VV}^{VBF}$  and  $\mu_{\tau\tau}^{VBF}$  match the experimental data very well. Compared to the SM, the theoretical calculations of new physics better conform to the experimental results. In addition, the calculation result of the signal strengths  $\mu_{ff}^{VBF}$  of  $h \rightarrow f\bar{f}$  are almost the same when  $\theta_{\lambda_T}$  takes different values, we analyze that this is because the triplets are uncoupled with fermions in the Lagrangian.

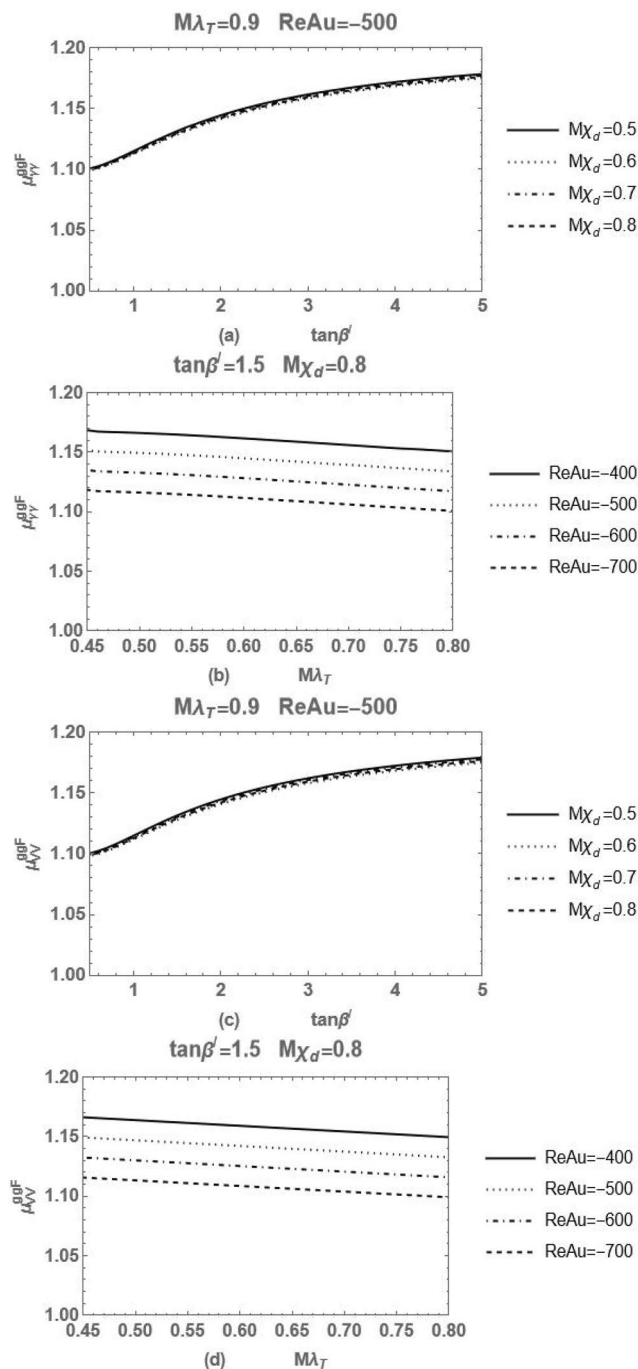


**Fig. 6.** (a, b) The variation of the signal strength  $\mu_{\gamma\gamma}^{ggF}$  and  $\mu_{VV}^{ggF}$  with  $\tan\beta'$  when  $M\chi_d$  is selected as different values. (c, d) The variation of the signal strength  $\mu_{\gamma\gamma}^{ggF}$  and  $\mu_{VV}^{ggF}$  with  $M\lambda_T$  when  $\text{Re}A_u$  is selected as different values.

Moreover, we explore the effects of some parameters that beyond the MSSM on Higgs mass and decay signal strengths, such as  $\tan\beta'$ ,  $\theta_{\chi_d}$ ,  $\theta_{\lambda_T}$ ,  $M\chi_d$  and  $M\lambda_T$ . From the Chapter IV, it can be seen that  $\theta_{\chi_d}$  and  $M\lambda_T$  are sensitive to Higgs decay signal strengths. In addition, in Chapter IV, we calculate the EDM of electrons and neutrons, as well as the mass spectrum of doubly charged particles, which well meet the experimental limitations. We also discuss the contribution of doubly charged particles to Higgs decay in the “Numerical analysis” Section. Due to the large mass of  $h^{++}$  and small  $v_t$ , the contribution of doubly charged particles to Higgs decay is relatively small. We look forward to more experimental measurements of these decays in the future, which will be beneficial for understanding more about the properties of Higgs boson.

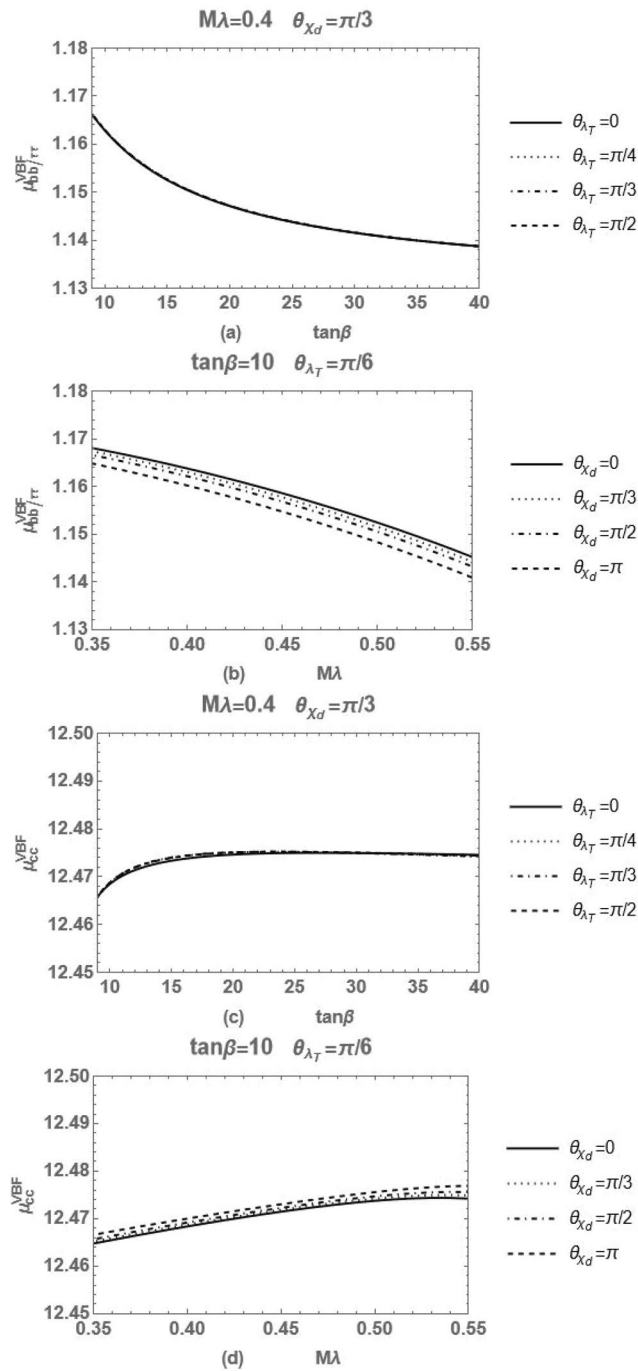


**Fig. 7.** (a, b) The variation of the signal strength  $\mu_{bb}^{VBF}$ ,  $\mu_{\tau\tau}^{VBF}$  and  $\mu_{cc}^{VBF}$  with  $\tan\beta$  when  $\theta_{\lambda_T}$  is selected as different phase angles. (c, d) The variation of the signal strength  $\mu_{bb}^{VBF}$ ,  $\mu_{\tau\tau}^{VBF}$  and  $\mu_{cc}^{VBF}$  with  $M\lambda$  when  $\theta_{\chi_d}$  is selected as different phase angles.

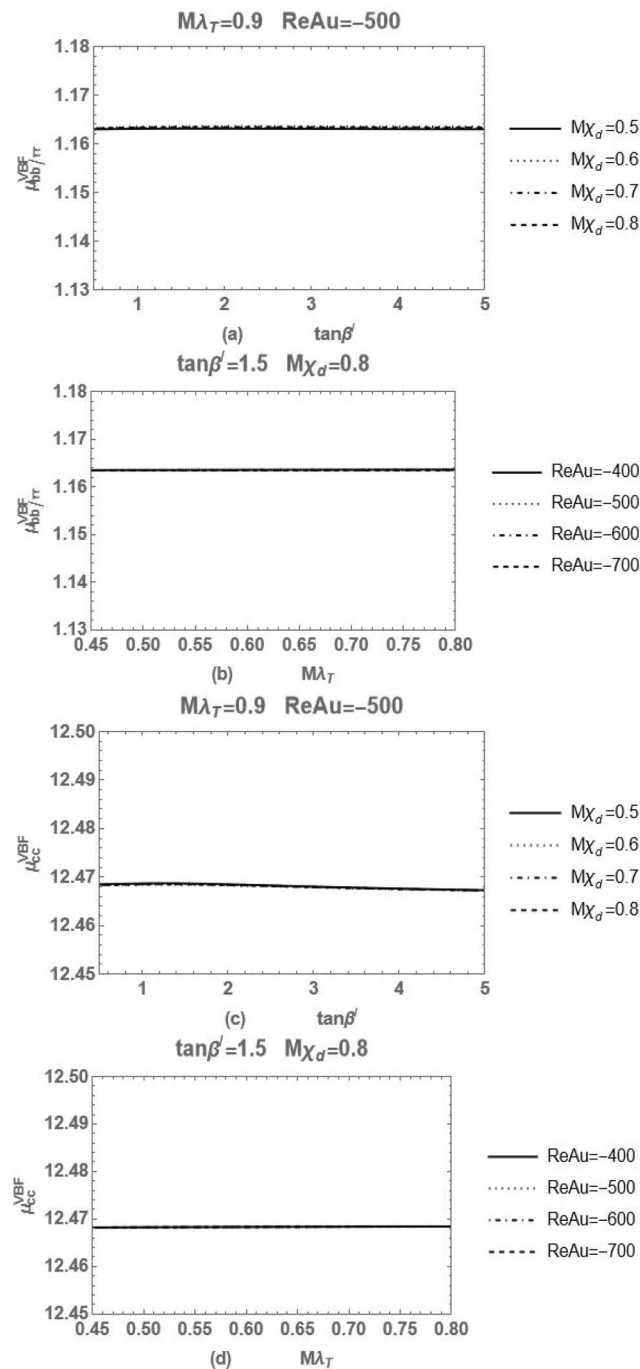


**Fig. 8.** (a, b) The variation of the signal strength  $\mu_{bb}^{VBF}$ ,  $\mu_{\tau\tau}^{VBF}$  and  $\mu_{cc}^{VBF}$  with  $\tan\beta'$  when  $M\chi_d$  is selected as different values. (c, d) The variation of the signal strength  $\mu_{bb}^{VBF}$ ,  $\mu_{\tau\tau}^{VBF}$  and  $\mu_{cc}^{VBF}$  with  $M\lambda_T$  when  $\text{Re}A_u$  is selected as different values.

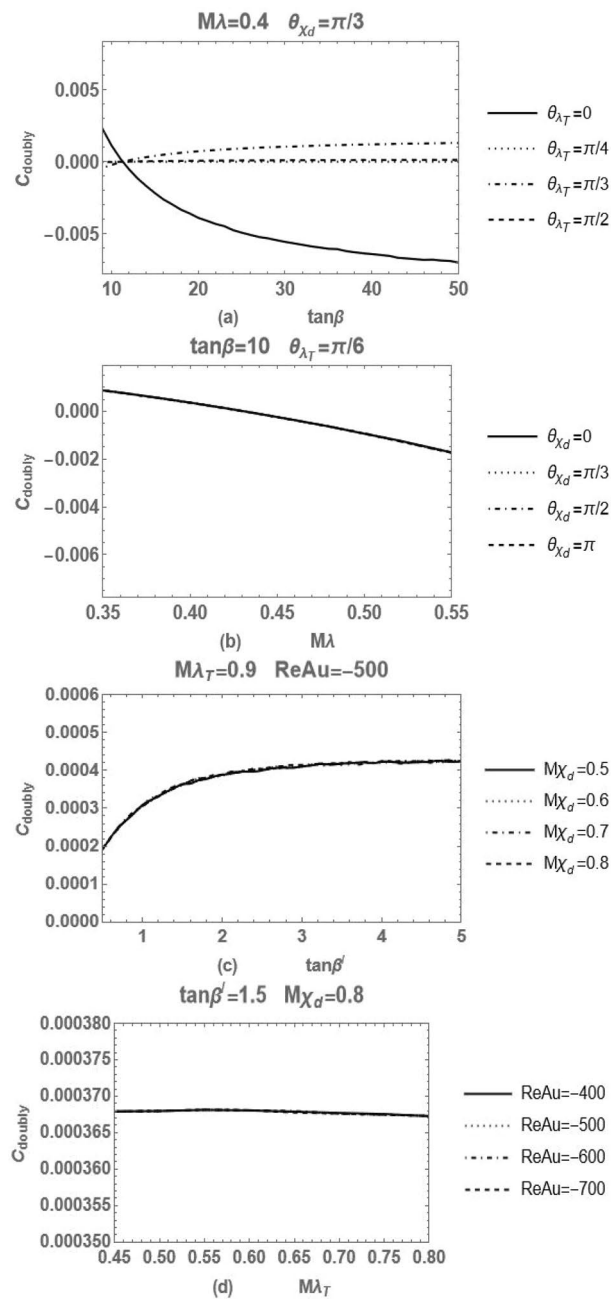


**Fig. 9.** (a) The variation of  $C_{\text{doubly}}$  with  $\tan\beta$  when  $\theta_{\lambda_T}$  is selected as different phase angles. (b) The variation of  $C_{\text{doubly}}$  with  $M\lambda$  when  $\theta_{\chi_d}$  is selected as different phase angles. (c) The variation of  $C_{\text{doubly}}$  with  $\tan\beta'$  when  $M\chi_d$  is selected as different values. (d) The variation of  $C_{\text{doubly}}$  with  $M\lambda_T$  when  $\text{Re}A_u$  is selected as different values.



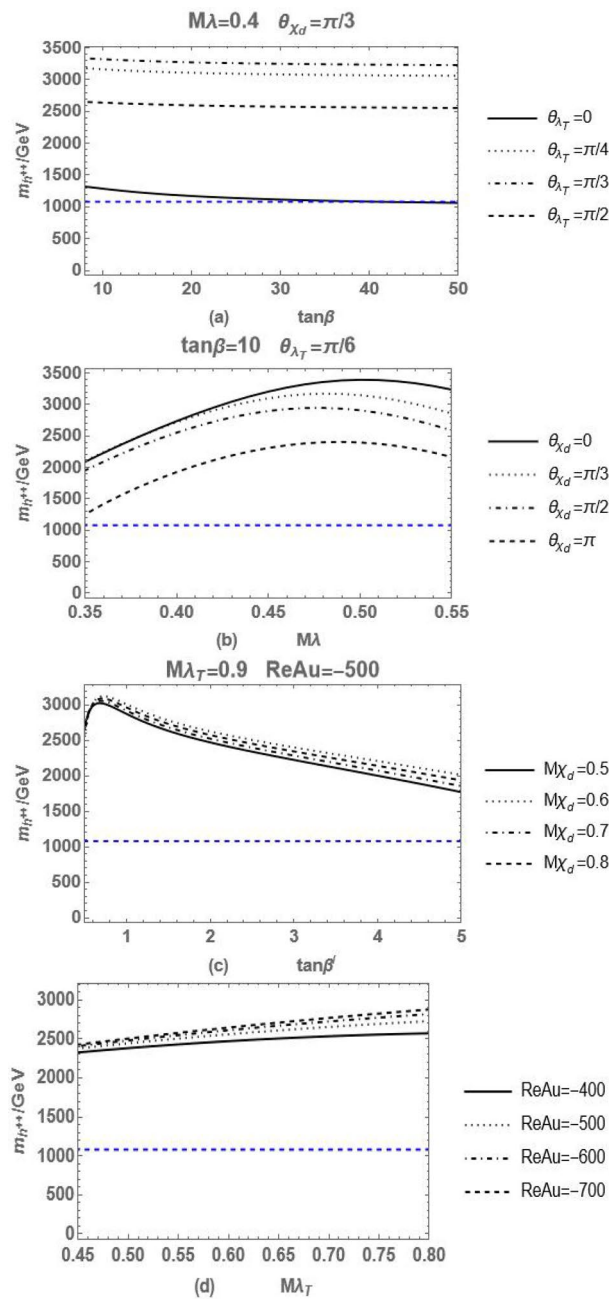


**Fig. 10.** (a) The variation of the mass of  $h^{++}$  with  $\tan\beta$  when  $\theta_{\lambda_T}$  is selected as different phase angles. (b) The variation of the mass of  $h^{++}$  with  $M\lambda$  when  $\theta_{\chi_d}$  is selected as different phase angles. (c) The variation of the mass of  $h^{++}$  with  $\tan\beta'$  when  $M\chi_d$  is selected as different values. (d) The variation of the mass of  $h^{++}$  with  $M\lambda_T$  when  $\text{Re}A_u$  is selected as different values.

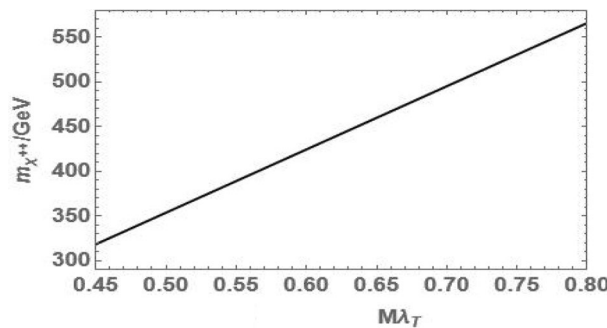


**Fig. 11.** The variation of the mass of  $\chi^{++}$  with  $M\lambda_T$ .

## Data availability

All data generated or analysed during this study are included in this published article.

Received: 25 April 2024; Accepted: 26 August 2024

Published online: 04 September 2024

## References

- Weinberg, S. A model of leptons. *Phys. Rev. Lett.* **19**, 1264. <https://doi.org/10.1103/PhysRevLett.19.1264> (1967).
- Glashow, S. L. Partial symmetries of weak interactions. *Nucl. Phys.* **22**, 579. [https://doi.org/10.1016/0029-5582\(61\)90469-2](https://doi.org/10.1016/0029-5582(61)90469-2) (1961).
- Aad, G. *et al.* Observation of a new particle in the search for the Standard Model Higgs Boson with the ATLAS detector at the LHC. *Phys. Lett. B* **716**, 1. <https://doi.org/10.1016/j.physletb.2012.08.020> (2012).
- Chatrchyan, S. *et al.* Observation of a New Boson at a mass of 125 GeV with the CMS experiment at the LHC. *Phys. Lett. B* **716**, 30. <https://doi.org/10.1016/j.physletb.2012.08.021> (2012).
- Abe, K. *et al.* Indication of electron neutrino appearance from an accelerator-produced off-axis muon neutrino beam. *Phys. Rev. Lett.* **107**, 041801. <https://doi.org/10.1103/PhysRevLett.107.041801> (2011).
- Adamson, P. *et al.* Improved search for muon-neutrino to electron-neutrino oscillations in MINOS. *Phys. Rev. Lett.* **107**, 181802. <https://doi.org/10.1103/PhysRevLett.107.181802> (2011).
- Rosiek, J. Complete set of Feynman rules for the minimal supersymmetric extension of the standard model. *Phys. Rev. D* **41**, 3464. <https://doi.org/10.1103/PhysRevD.41.3464> (1990).
- Kim, J. E. & Nilles, H. P. The mu problem and the strong CP problem. *Phys. Lett. B* **138**, 150. [https://doi.org/10.1016/0370-2693\(84\)91890-2](https://doi.org/10.1016/0370-2693(84)91890-2) (1984).
- Ellwanger, U., Hugonie, C. & Teixeira, A. M. The next-to-minimal supersymmetric standard model. *Phys. Rept.* **496**, 1. <https://doi.org/10.1016/j.physrep.2010.07.001> (2010).
- Mason, J. D. Gauge Mediation with a small mu term and light Squarks. *Phys. Rev. D* **80**, 015026. <https://doi.org/10.1103/PhysRevD.80.015026> (2009).
- Ellwanger, U. & Hugonie, C. The Upper bound on the lightest Higgs mass in the NMSSM revisited. *Mod. Phys. Lett. A* **22**, 1581. <https://doi.org/10.1142/S0217732307023870> (2007).
- Ananthanarayan, B. & Pandita, P. N. Particle spectrum in the nonminimal supersymmetric standard model with tan beta approximately = m(t)/m(b). *Phys. Lett. B* **371**, 245 (1996).
- Ananthanarayan, B. & Pandita, P. N. The Nonminimal supersymmetric standard model at large tan beta. *Int. J. Mod. Phys. A* **12**, 2321. <https://doi.org/10.1142/S0217751X97001353> (1997).
- Ellwanger, U. & Hugonie, C. Yukawa induced radiative corrections to the lightest Higgs boson mass in the NMSSM. *Phys. Lett. B* **623**, 93. <https://doi.org/10.1016/j.physletb.2005.07.039> (2005).
- Degrassi, G. & Slavich, P. On the radiative corrections to the neutral Higgs boson masses in the NMSSM. *Nucl. Phys. B* **825**, 119. <https://doi.org/10.1016/j.nuclphysb.2009.09.018> (2010).
- Agashe, K., Azatov, A., Katz, A. & Kim, D. Improving the tunings of the MSSM by adding triplets and singlet. *Phys. Rev. D* **84**, 115024. <https://doi.org/10.1103/PhysRevD.84.115024> (2011).
- Espinoza, J. R. & Quiros, M. Higgs triplets in the supersymmetric standard model. *Nucl. Phys. B* **384**, 113. [https://doi.org/10.1016/0550-3213\(92\)90464-M](https://doi.org/10.1016/0550-3213(92)90464-M) (1992).
- Zhang, Z.-Y., Yang, J.-L., Zhang, H.-B. & Feng, T.-F. Transition magnetic moment of Majorana neutrinos in the triplets next-to-minimal MSSM. [arXiv:2406.18323](https://arxiv.org/abs/2406.18323) [hep-ph] (2024).
- Christenson, J. H., Cronin, J. W., Fitch, V. L. & Turlay, R. Evidence for the  $2\pi$  Decay of the  $K_2^0$  Meson. *Phys. Rev. Lett.* **13**, 138. <https://doi.org/10.1103/PhysRevLett.13.138> (1964).
- Neubert, M. B decays and CP violation. *Int. J. Mod. Phys. A* **11**, 4173. <https://doi.org/10.1142/S0217751X96001966> (1996).
- Sakharov, A. D. Violation of CP Invariance, C asymmetry, and baryon asymmetry of the universe. *Pisma Zh. Eksp. Teor. Fiz.* **5**, 32. <https://doi.org/10.1070/PU1991v034n05ABEH002497> (1967).
- Lee, T. D. A theory of spontaneous T violation. *Phys. Rev. D* **8**, 1226. <https://doi.org/10.1103/PhysRevD.8.1226> (1973).
- Weinberg, S. Gauge theory of CP violation. *Phys. Rev. Lett.* **37**, 657. <https://doi.org/10.1103/PhysRevLett.37.657> (1976).
- Coleman, S. R. & Weinberg, E. J. Radiative corrections as the origin of spontaneous symmetry breaking. *Phys. Rev. D* **7**, 1888. <https://doi.org/10.1103/PhysRevD.7.1888> (1973).
- Carena, M., Espinoza, J. R., Quiros, M. & Wagner, C. E. M. Analytical expressions for radiatively corrected Higgs masses and couplings in the MSSM. *Phys. Lett. B* **355**, 209. [https://doi.org/10.1016/0370-2693\(95\)00694-G](https://doi.org/10.1016/0370-2693(95)00694-G) (1995).
- Carena, M., Quiros, M. & Wagner, C. E. M. Effective potential methods and the Higgs mass spectrum in the MSSM. *Nucl. Phys. B* **461**, 407. [https://doi.org/10.1016/0550-3213\(95\)00665-6](https://doi.org/10.1016/0550-3213(95)00665-6) (1996).
- Carena, M., Ellis, J. R., Pilaftsis, A. & Wagner, C. E. M. Renormalization group improved effective potential for the MSSM Higgs sector with explicit CP violation. *Nucl. Phys. B* **586**, 92. [https://doi.org/10.1016/S0550-3213\(00\)00358-8](https://doi.org/10.1016/S0550-3213(00)00358-8) (2000).
- Chen, H.-X., Cui, S.-K., Zhu, N.-Y., Zhang, Z.-Y. & Hu, H.-C. B meson rare decays in the TMSSM\*. *Chin. Phys. C* **48**, 053104. <https://doi.org/10.1088/1674-1137/ad2a62> (2024).

29. Hu, H.-C. Zhang, Z.-Y. Zhu, N.-Y. & Chen, H.-X. Higgs boson decays  $h \rightarrow MZ$  in the TNMSSM. [arXiv:2406.00946](#) [hep-ph] (2024).
30. Ouahid, M. A. & Ahl Laamara, R. Neutrino and doubly charged Higgs boson phenomenology in flavored-TNMSSM. *Nucl. Phys. B* **974**, 115640. <https://doi.org/10.1016/j.nuclphysb.2021.115640> (2022).
31. Carena, M., Gori, S., Shah, N. R. & Wagner, C. E. M. A 125 GeV SM-like Higgs in the MSSM and the  $\gamma\gamma$  rate. *J. High Energy Phys.* **03**, 014 (2012).
32. Oshimo, N. Coexistence of CP eigenstates in Higgs boson decay. *Prog. Theor. Exp. Phys.* **2013**, 083B04. <https://doi.org/10.1093/ptep/ptt062> (2013).
33. Ellis, J. R., Gaillard, M. K. & Nanopoulos, D. V. A phenomenological profile of the Higgs Boson. *Nucl. Phys. B* **106**, 292. [https://doi.org/10.1016/0550-3213\(76\)90382-5](https://doi.org/10.1016/0550-3213(76)90382-5) (1976).
34. Djouadi, A. The Anatomy of electro-weak symmetry breaking. II. The Higgs bosons in the minimal supersymmetric model. *Phys. Rept.* **459**, 1. <https://doi.org/10.1016/j.physrep.2007.10.005> (2008).
35. Gunion, J. F. & Haber, H. E. Errata for Higgs bosons in supersymmetric models: 1, 2 and 3. [arXiv:hep-ph/9301205](#) (1992).
36. Wilczek, F. Decays of heavy vector mesons into Higgs particles. *Phys. Rev. Lett.* **39**, 1304. <https://doi.org/10.1103/PhysRevLett.39.1304> (1977).
37. Georgi, H. M., Glashow, S. L., Machacek, M. E. & Nanopoulos, D. V. Higgs bosons from two gluon annihilation in proton proton collisions. *Phys. Rev. Lett.* **40**, 692. <https://doi.org/10.1103/PhysRevLett.40.692> (1978).
38. Kileng, B. Effects of scalar mixing in  $g \rightarrow \text{Higgs} \rightarrow \text{gamma gamma}$ . *Z. Phys. C* **63**, 87. <https://doi.org/10.1007/BF01577547> (1994).
39. Djouadi, A. Squark effects on Higgs boson production and decay at the LHC. *Phys. Lett. B* **435**, 101. [https://doi.org/10.1016/S0370-2693\(98\)00784-9](https://doi.org/10.1016/S0370-2693(98)00784-9) (1998).
40. Belanger, G., Boudjema, F., Donato, F., Godbole, R. & Rosier-Lees, S. SUSY Higgs at the LHC: Effects of light charginos and neutralinos. *Nucl. Phys. B* **581**, 3. [https://doi.org/10.1016/S0550-3213\(00\)00243-1](https://doi.org/10.1016/S0550-3213(00)00243-1) (2000).
41. Shifman, M. A., Vainshtein, A. I., Voloshin, M. B. & Zakharov, V. I. Low-energy theorems for Higgs boson couplings to photons. *Sov. J. Nucl. Phys.* **30**, 711 (1979).
42. Gavela, M. B., Girardi, G., Malleville, C. & Sorba, P. A nonlinear R(xi) gauge condition for the electroweak SU(2) X U(1) model. *Nucl. Phys. B* **193**, 257. [https://doi.org/10.1016/0550-3213\(81\)90529-0](https://doi.org/10.1016/0550-3213(81)90529-0) (1981).
43. Kalyniak, P., Bates, R. & Ng, J. N. Two photon decays of scalar and pseudoscalar bosons in supersymmetry. *Phys. Rev. D* **33**, 755. <https://doi.org/10.1103/PhysRevD.33.755> (1986).
44. Bates, R., Ng, J. N. & Kalyniak, P. Two photon decay widths of Higgs bosons in minimal broken supersymmetry. *Phys. Rev. D* **34**, 172. <https://doi.org/10.1103/PhysRevD.34.172> (1986).
45. Kane, G. L., Kribs, G. D., Martin, S. P. & Wells, J. D. Two photon decays of the lightest Higgs boson of supersymmetry at the LHC. *Phys. Rev. D* **53**, 213. <https://doi.org/10.1103/PhysRevD.53.213> (1996).
46. Djouadi, A., Driesen, V., Hollik, W. & Illana, J. I. The Coupling of the lightest SUSY Higgs boson to two photons in the decoupling regime. *Eur. Phys. J. C* **1**, 149. <https://doi.org/10.1007/BF01245805> (1998).
47. Gunion, J. F., Haber, H. E., Kane, G. L. & Dawson, S. *The Higgs Hunter's Guide* (CRC Press, 2000).
48. Lee, B. W., Quigg, C. & Thacker, H. B. Weak interactions at very high-energies: The role of the Higgs boson mass. *Phys. Rev. D* **16**, 1519. <https://doi.org/10.1103/PhysRevD.16.1519> (1977).
49. Resnick, L., Sundaresan, M. K. & Watson, P. J. S. Is there a light scalar boson?. *Phys. Rev. D* **8**, 172. <https://doi.org/10.1103/PhysRevD.8.172> (1973).
50. Rizzo, T. G. Decays of heavy Higgs bosons. *Phys. Rev. D* **22**, 722. <https://doi.org/10.1103/PhysRevD.22.722> (1980).
51. Pocsik, G. & Torma, T. On the decays of heavy Higgs bosons. *Z. Phys. C* **6**, 1. <https://doi.org/10.1007/BF01427913> (1980).
52. Keung, W.-Y. & Marciano, W. J. Higgs scalar decays:  $H \rightarrow W^+ X$ . *Phys. Rev. D* **30**, 248. <https://doi.org/10.1103/PhysRevD.30.248> (1984).
53. Cahn, R. N. The Higgs boson. *Rept. Prog. Phys.* **52**, 389. <https://doi.org/10.1088/0034-4885/52/4/001> (1989).
54. Grau, A., Panchieri, G. & Phillips, R. J. N. Contributions of off-shell top quarks to decay processes. *Phys. Lett. B* **251**, 293. [https://doi.org/10.1016/0370-2693\(90\)90939-4](https://doi.org/10.1016/0370-2693(90)90939-4) (1990).
55. Kniehl, B. A. The Higgs boson decay  $H \rightarrow Z gg$ . *Phys. Lett. B* **244**, 537. [https://doi.org/10.1016/0370-2693\(90\)90360-1](https://doi.org/10.1016/0370-2693(90)90360-1) (1990).
56. Arbey, A., Deandrea, A., Mahmoudi, F. & Tarhini, A. Anomaly mediated supersymmetric models and Higgs data from the LHC. *Phys. Rev. D* **87**, 115020. <https://doi.org/10.1103/PhysRevD.87.115020> (2013).
57. Workman, R. L. *et al.* Particle data group. *Rev. Part. Phys.* **2022**, 083C01 (2022).
58. Ibrahim, T. & Nath, P. The Neutron and the lepton EDMs in MSSM, large CP violating phases, and the cancellation mechanism. *Phys. Rev. D* **58**, 111301. <https://doi.org/10.1103/PhysRevD.58.111301> (1998). [Note [Erratum: *Phys. Rev. D* **60**, 099902 (1999)]].
59. Ibrahim, T., Itani, A. & Nath, P. Electron electric dipole moment as a sensitive probe of PeV scale physics. *Phys. Rev. D* **90**, 055006. <https://doi.org/10.1103/PhysRevD.90.055006> (2014).
60. Aboubrahim, A., Ibrahim, T., Nath, P. & Zorik, A. Chromoelectric dipole moments of quarks in MSSM extensions. *Phys. Rev. D* **92**, 035013. <https://doi.org/10.1103/PhysRevD.92.035013> (2015).
61. Yang, J.-L., Feng, T.-F. & Zhang, H.-B. Electroweak baryogenesis and electron EDM in the B-LSSM. *Eur. Phys. J. C* **80**, 210. <https://doi.org/10.1140/epjc/s10052-020-7753-9> (2020).
62. Yang, J.-L. *et al.* Electric dipole moments of neutron and heavy quarks in the B-LSSM. *J. High Energy Phys.* **04**, 013. [https://doi.org/10.1007/JHEP04\(2020\)013](https://doi.org/10.1007/JHEP04(2020)013) (2020).
63. Sirunyan, A. M. *et al.* Measurements of Higgs boson properties in the diphoton decay channel in proton-proton collisions at  $\sqrt{s} = 13$  TeV. *J. High Energy Phys.* **11**, 185. [https://doi.org/10.1007/JHEP11\(2018\)185](https://doi.org/10.1007/JHEP11(2018)185) (2018).
64. Aaboud, M. *et al.* Measurements of Higgs boson properties in the diphoton decay channel with 36 fb<sup>-1</sup> of  $pp$  collision data at  $\sqrt{s} = 13$  TeV with the ATLAS detector. *Phys. Rev. D* **98**, 052005. <https://doi.org/10.1103/PhysRevD.98.052005> (2018).
65. Aad, G. *et al.* Measurements of the Higgs boson production and decay rates and constraints on its couplings from a combined ATLAS and CMS analysis of the LHC  $pp$  collision data at  $\sqrt{s} = 7$  and 8 TeV. *J. High Energy Phys.* **08**, 045. [https://doi.org/10.1007/JHEP08\(2016\)045](https://doi.org/10.1007/JHEP08(2016)045) (2016).
66. Aaltonen, T. *et al.* Higgs boson studies at the Tevatron. *Phys. Rev. D* **88**, 052014. <https://doi.org/10.1103/PhysRevD.88.052014> (2013).
67. Aaboud, M. *et al.* Measurement of the Higgs boson coupling properties in the  $H \rightarrow ZZ^* \rightarrow 4\ell$  decay channel at  $\sqrt{s} = 13$  TeV with the ATLAS detector. *J. High Energy Phys.* **03**, 095. [https://doi.org/10.1007/JHEP03\(2018\)095](https://doi.org/10.1007/JHEP03(2018)095) (2018).
68. Sirunyan, A. M. *et al.* Measurements of properties of the Higgs boson decaying into the four-lepton final state in  $pp$  collisions at  $\sqrt{s} = 13$  TeV. *J. High Energy Phys.* **11**, 047. [https://doi.org/10.1007/JHEP11\(2017\)047](https://doi.org/10.1007/JHEP11(2017)047) (2017).
69. Sirunyan, A. M. *et al.* Observation of Higgs boson decay to bottom quarks. *Phys. Rev. Lett.* **121**, 121801. <https://doi.org/10.1103/PhysRevLett.121.121801> (2018).
70. Aaboud, M. *et al.* Observation of  $H \rightarrow b\bar{b}$  decays and  $VH$  production with the ATLAS detector. *Phys. Lett. B* **786**, 59. <https://doi.org/10.1016/j.physletb.2018.09.013> (2018).
71. Tumasyan, A. *et al.* Search for Higgs boson decay to a charm quark-antiquark pair in proton-proton collisions at  $s = 13$  TeV. *Phys. Rev. Lett.* **131**, 061801. <https://doi.org/10.1103/PhysRevLett.131.061801> (2023).

72. Tumasyan, A. *et al.* Search for Higgs boson and observation of Z boson through their decay into a charm quark-antiquark pair in boosted topologies in proton-proton collisions at  $\sqrt{s} = 13$  TeV. *Phys. Rev. Lett.* **131**, 041801. <https://doi.org/10.1103/PhysRevLett.131.041801> (2023).
73. Sirunyan, A. M. *et al.* Observation of the Higgs boson decay to a pair of  $\tau$  leptons with the CMS detector. *Phys. Lett. B* **779**, 283. <https://doi.org/10.1016/j.physletb.2018.02.004> (2018).
74. Novak, T. Searches for singly- and doubly-charged Higgs bosons with the ATLAS detector. <https://doi.org/10.22323/1.449.0433> (2024)
75. Aad, G. *et al.* Search for doubly charged Higgs boson production in multi-lepton final states using  $139 \text{ fb}^{-1}$  of proton-proton collisions at  $\sqrt{s} = 13$  TeV with the ATLAS detector. *Eur. Phys. J. C* **83**, 605. <https://doi.org/10.1140/epjc/s10052-023-11578-9> (2023).
76. Leban, B. Search for doubly charged Higgs boson production in multi-lepton final states using  $139 \text{ fb}^{-1}$  of proton-proton collisions at  $\sqrt{s} = 13$  TeV with the ATLAS detector. <https://doi.org/10.22323/1.414.1081> (2022)

## Acknowledgements

The work has been supported by Natural Science Foundation of Guangxi Autonomous Region with Grant No. 2022GXNSFDA035068.

## Author contributions

N.Z. wrote the main manuscript text, H.C. and H.H. prepared figures 1–2. All authors reviewed the manuscript.

## Competing interests

The authors declare no competing interests.

## Additional information

**Supplementary Information** The online version contains supplementary material available at <https://doi.org/10.1038/s41598-024-71222-8>.

**Correspondence** and requests for materials should be addressed to N.-Y.Z.

**Reprints and permissions information** is available at [www.nature.com/reprints](http://www.nature.com/reprints).

**Publisher's note** Springer Nature remains neutral with regard to jurisdictional claims in published maps and institutional affiliations.

**Open Access** This article is licensed under a Creative Commons Attribution-NonCommercial-NoDerivatives 4.0 International License, which permits any non-commercial use, sharing, distribution and reproduction in any medium or format, as long as you give appropriate credit to the original author(s) and the source, provide a link to the Creative Commons licence, and indicate if you modified the licensed material. You do not have permission under this licence to share adapted material derived from this article or parts of it. The images or other third party material in this article are included in the article's Creative Commons licence, unless indicated otherwise in a credit line to the material. If material is not included in the article's Creative Commons licence and your intended use is not permitted by statutory regulation or exceeds the permitted use, you will need to obtain permission directly from the copyright holder. To view a copy of this licence, visit <http://creativecommons.org/licenses/by-nc-nd/4.0/>.

© The Author(s) 2024